

# Upconversion Nonlinear Structured Illumination Microscopy

Baolei Liu, Chaohao Chen, Xiangjun Di, Jiayan Liao, Shihui Wen, Qian Peter Su, Xuchen Shan, Zai-Quan Xu, Lining Arnold Ju, Chao Mi, Fan Wang,\* and Dayong Jin\*



Cite This: *Nano Lett.* 2020, 20, 4775–4781



Read Online

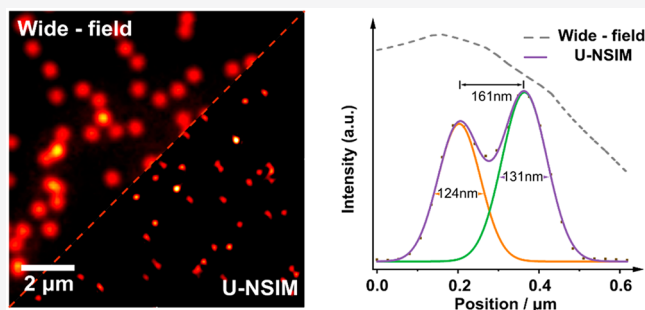
ACCESS |

Metrics & More

Article Recommendations

Supporting Information

**ABSTRACT:** Video-rate super-resolution imaging through biological tissue can visualize and track biomolecule interplays and transportations inside cellular organisms. Structured illumination microscopy allows for wide-field super resolution observation of biological samples but is limited by the strong extinction of light by biological tissues, which restricts the imaging depth and degrades its imaging resolution. Here we report a photon upconversion scheme using lanthanide-doped nanoparticles for wide-field super-resolution imaging through the biological transparent window, featured by near-infrared and low-irradiance nonlinear structured illumination. We demonstrate that the 976 nm excitation and 800 nm upconverted emission can mitigate the aberration. We found that the nonlinear response of upconversion emissions from single nanoparticles can effectively generate the required high spatial frequency components in the Fourier domain. These strategies lead to a new modality in microscopy with a resolution below 131 nm, 1/7th of the excitation wavelength, and an imaging rate of 1 Hz.



**KEYWORDS:** SIM, super-resolution, nonlinear, NIR, upconversion nanoparticles, deep tissue

## INTRODUCTION

Fluorescence microscopy has been widely used to visualize cellular structures, biomolecular distributions, and biological processes.<sup>1,2</sup> However, many subcellular structures, organelles, and molecular analytes are typically smaller than a few hundreds of nanometers, which cannot be resolved by conventional microscopy due to the optical diffraction limit. Super-resolution microscopy techniques, including stimulated emission depletion (STED) microscopy,<sup>3</sup> single molecule localization microscopy,<sup>4,5</sup> super-resolution optical fluctuation imaging (SOFI),<sup>6</sup> and structured illumination microscopy (SIM),<sup>7–9</sup> have been developed to bypass this limitation.

SIM typically requires closely spaced periodic patterns to down-modulate the high spatial frequency information in the sample so that with the support of optical transfer functions the high frequency information can be reconstructed from a series of images obtained from the patterned illuminations at various orientations. SIM typically offers the high-speed imaging with a resolution at around 1 of the excitation wavelength. When the high excitation power is used, the nonlinear saturated photoresponse can be explored to further improve the resolution of SIM in the regime of 50 nm<sup>10</sup> and resolve subcellular structures.<sup>11</sup> New advances made in the denoising process and modified excitation conditions have been applied to SIM, so that nonlinear SIM,<sup>10–12</sup> Hessian-SIM,<sup>13</sup> and grazing incidence SIM<sup>14</sup> have been recently developed with high imaging speed for the observations of

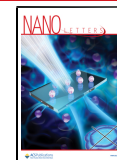
ultrastructures of cellular organelles and their structural dynamics, such as mitochondrial cristae.<sup>13</sup>

The next challenge is to apply these techniques for applications, like deep-tissue imaging and nanomedicine tracking, as the strong extinction aberrates the structured illumination patterns, introduces undesirable out-of-focus light, and decreases sample's emission intensity, deteriorating the imaging resolution and imaging speed.<sup>15</sup> To address this challenge, near-infrared excitation has been implemented to mitigate the aberration. Two-photon<sup>16</sup> or multiphoton excitation<sup>17</sup> in conjugation with spot scanning SIM has been reported to improve the imaging depth through tissue, but at the price of low speed caused by the spot scanning scheme (typically 1 Hz imaging rate for a 50 μm × 50 μm area). Organic fluorescent dyes and proteins are the most common imaging probes for SIM, because of their outstanding staining and specific targeting ability to organelles.<sup>8,13,18,19</sup> Nevertheless, these probes require the tightly focused and high-power pulsed laser to activate the multiphoton absorption process, due to their small multiphoton absorption cross-

**Received:** February 2, 2020

**Revised:** March 17, 2020

**Published:** March 25, 2020



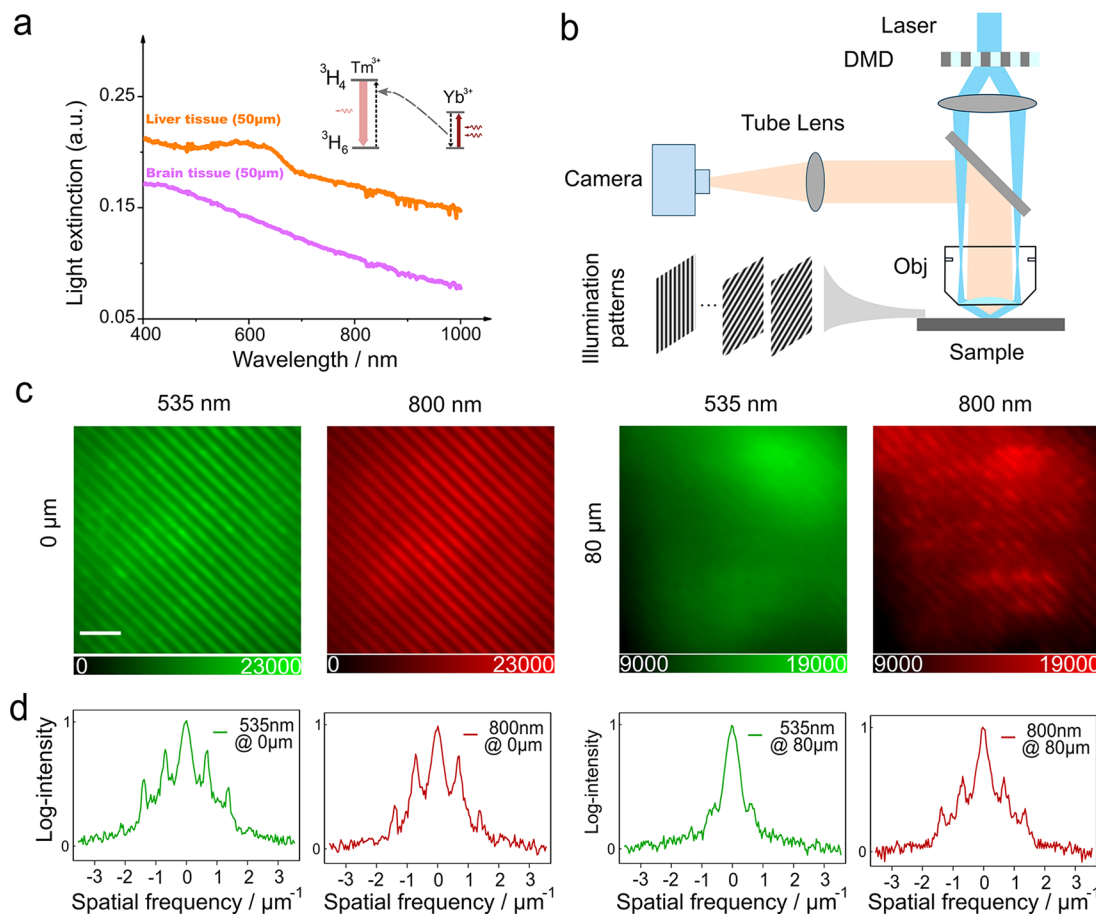


**Figure 1.** Scheme and advances of upconversion nonlinear SIM for super resolution imaging through thick tissues. (a) Light extinction spectra of 50  $\mu\text{m}$  thick mice brain and liver tissues, measured by a commercial ultraviolet–visible spectrophotometer. Inset: single lanthanide-doped UCNPs with a network of thousands of codoped ytterbium ions ( $\text{Yb}^{3+}$ ) as sensitizers and thulium ( $\text{Tm}^{3+}$ ) ions as activators can absorb 976 nm excitation photons and convert them into 800 nm emissions with nonlinear photoresponse. (b) Schematic diagram of the SIM setup. A digital mirror device (DMD) is used here to generate structured illumination patterns at the sample plane. The fluorescence image under the structured illumination is captured by an EMCCD. (c) Under the sinusoidal structured excitation at 976 nm, the comparison of fluorescence images collected through the emission bands of  $535 \pm 25$  and  $808 \pm 10$  nm without and with 80  $\mu\text{m}$  thick brain tissues. For comparison purposes, the emission intensities from the same sample area through the bands of 535 and 800 nm have been adjusted to reach the same level by tuning the excitation power. Scale bar: 5  $\mu\text{m}$ . (d) Line profiles of Fourier spectra (on a logarithmic scale) of the diagonal cross section profiles in (c).

section.<sup>20</sup> The required high excitation power, especially by nonlinear SIM, limits the long-duration visualization of subcellular structure in living cells.

Upconversion nanoparticles (UCNPs) are an emerging near-infrared (NIR) imaging probe for optical imaging. UCNPs contain multiple lanthanide sensitizer ions to absorb NIR photons and activator ions to upconvert photon energy and emit light, and both types of ions have multiple long-lived intermediate excited states and can be highly doped in the typical fluoride nanocrystal host. Hence, these nanoparticles can effectively absorb NIR photons and sequentially convert them into the shorter wavelength ultraviolet, visible, and NIR photons through the nonlinear energy transfer process.<sup>21,22</sup> Benefiting from their unique nonlinear response, nonbleaching nonblinking photostability, and anti-Stoke excitation–emission properties,<sup>23–27</sup> UCNPs have been recently discovered as a new library of super-resolution imaging<sup>28–32</sup> and single molecule tracking probes.<sup>23,27,33</sup> We have recently demonstrated a near-infrared emission saturation nanoscopy method that can detect single nanocrystals through 93  $\mu\text{m}$  thick tissue with 50 nm resolution.<sup>29,34</sup> However, these super-resolution imaging modalities require focused doughnut beam excitations

that suffer from low scanning rates and therefore are not suitable for fast super-resolution imaging.

Here we report a strategy of upconversion nonlinear SIM (U-NSIM) toward fast super-resolution imaging through thick biological tissues. We apply ytterbium ( $\text{Yb}^{3+}$ ) and thulium ( $\text{Tm}^{3+}$ ) codoped UCNPs as the imaging probe that emits upconverted NIR emissions at 800 nm upon NIR excitation at 976 nm, both within the transparent biological window, to extend the imaging penetration depth. Setting the 976 nm structured pattern excitation can not only mitigate the aberration on the pattern but also easily activate UCNPs to emit bright NIR photons. The unique nonlinear photoresponse of UCNPs enables the onset of an efficient nonlinear mode on SIM for obtaining higher-frequency imaging resolution. We further demonstrate that fine-tuning of the doping concentrations in UCNPs can modify the nonlinearity of the photon response and to further improve the optical resolution to 1/7th of the excitation wavelength.

## RESULTS AND DISCUSSION

To evaluate the upconversion strategy to achieve fast super-resolution imaging through thick tissues, we first examine the

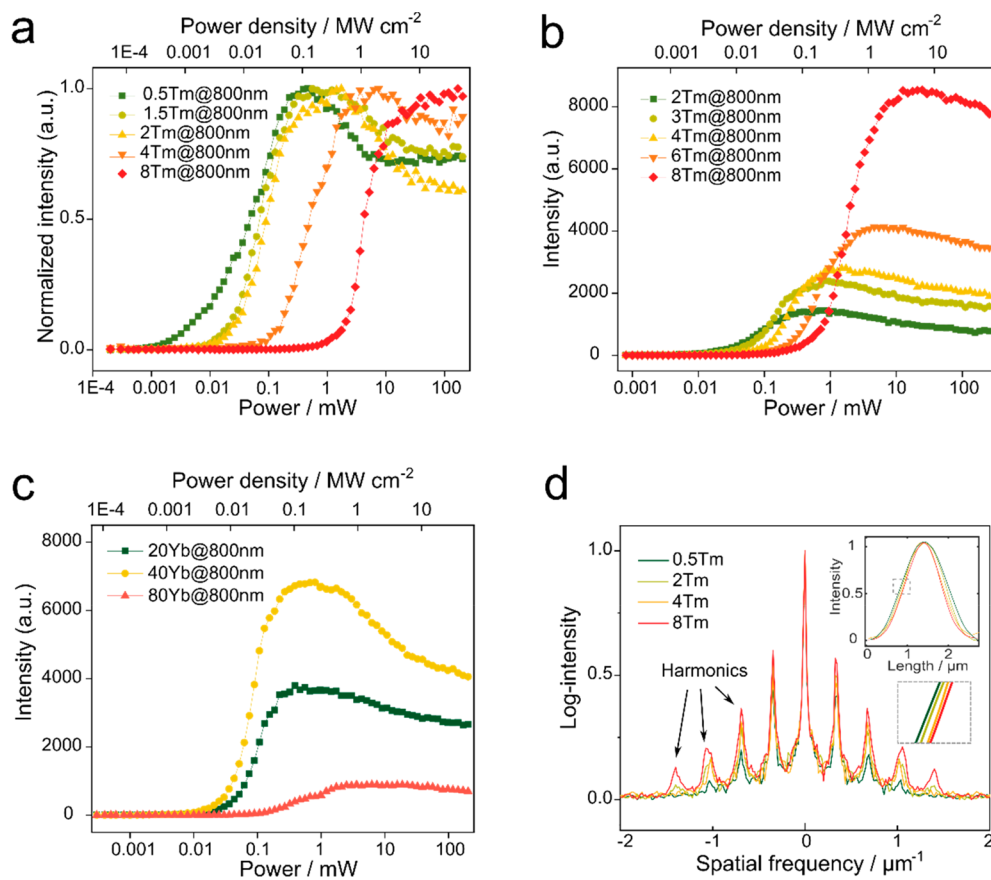


**Figure 2.** Saturation intensity curves of the 800 nm emissions from single UCNPs. (a) Normalized emission saturation curves of a single UCNP ( $\text{NaYF}_4$ : 20%  $\text{Yb}^{3+}$ ,  $x\%$   $\text{Tm}^{3+}$  nanoparticles,  $x = 0.5, 1.5, 2, 4$ , and  $8$ ) under 976 nm excitation. (b) 800 nm emission saturation curves obtained for a single UCNP ( $\text{NaYF}_4$ : 20%  $\text{Yb}^{3+}$ ,  $x\%$   $\text{Tm}^{3+}$  nanoparticles,  $x = 2, 3, 4, 6$ , and  $8$ ). (c) 800 nm emission saturation curves obtained for a single UCNP. ( $\text{NaYF}_4$ :  $x\%$   $\text{Yb}^{3+}$ , 4%  $\text{Tm}^{3+}$  nanoparticles,  $x = 20, 40$ , and  $80$ ) (d) Fourier transforms corresponding to the intensity profiles measured with different doped UCNPs. The inset (right middle) shows the cross section profiles of measured emission patterns.

light penetration depths for the UCNPs' multicolor emissions. Under the continuous wave (CW) excitation condition at a power density of  $\sim 10 \text{ kW/cm}^2$ , UCNPs can effectively convert the energy from 976 nm photons into the two-photon state  ${}^3\text{H}_4$  that emits 800 nm photons (Supplementary Note 3 and Figure S2), where the tissue has less extinction. Figure 1a shows the light extinction spectra of the  $50 \mu\text{m}$  thick mouse brain and liver tissue slices, which shows better penetration ability for the 800 nm emission and 976 nm excitation compared with that in the visible wavelength range. Figure 1c shows the comparison penetration abilities of structured patterns at 535 and 800 nm emission bands. In this experiment, we mix the two types of UCNPs ( $\text{NaYF}_4$ : 2%  $\text{Er}^{3+}$ , 20%  $\text{Yb}^{3+}$  and  $\text{NaYF}_4$ : 2%  $\text{Tm}^{3+}$ , 20%  $\text{Yb}^{3+}$ ) and uniformly disperse them onto the glass slide (Supplementary Note 1 and 2). Then we use a 976 nm sinusoidal structured pattern to excite the layer of UCNPs and image the emission patterns (Figure 1b, Supplementary Note 4, and Figure S4). Without the tissue, marked as  $0 \mu\text{m}$ , both 535 nm (from  $\text{Er}^{3+}$ ) and 800 nm (from  $\text{Tm}^{3+}$ ) emissions produce the desirable structured emission patterns. When an  $80 \mu\text{m}$  tissue slice is placed on top of the UCNPs layer, the 535 nm emission pattern is heavily distorted and almost loses its structure information, while the 800 nm emission pattern mitigates the scattering and well keeps its pattern. We further quantify the information preserved in the emission patterns by Fourier domain image analysis (Figure 1d). Both the diagonal cross

sections of the Fourier spectra of the emission patterns from two bands at  $0 \mu\text{m}$  show clear peaks, indicating sufficient ability to transfer the designed spatial frequencies. However, the 535 nm emission pattern loses this spatial information with the  $80 \mu\text{m}$  tissue, while the 800 nm emission pattern well keeps the spatial information. This indicates that the upconversion SIM method using both 976 excitation and 800 emission bands at NIR is superior to visible emissions as it can send and detect the structured excitation and emission patterns through the thick tissue.

SIM operated in the linear response regime of the fluorescence probes generally enhances the resolution by a factor of approximately 2, compared with that in wide-field microscopy. Nonlinear operation of SIM requires high excitation power density for the probes to produce nonlinear photoresponses, e.g., fluorescence saturation<sup>10</sup> and fluorophore depletion,<sup>11,12</sup> to surpass the resolution limitation of linear SIM. Nonlinear SIM can theoretically produce an unlimited factor of enhancement on the imaging resolution.<sup>10</sup> The photon upconversion process is a typical nonlinear process as it requires multiphoton excitation to emit the multicolor upconversion emissions from ladderlike multi-metastable excited states of rare-earth ions. We first measure the 800 nm emission saturation curves from single nanoparticles (Supplementary Notes 1–3 and Figure S3). Figure 2a shows the obvious nonlinear photoresponse behaviors of UCNPs, and the nonlinearity (the rising-up slope) increases with the

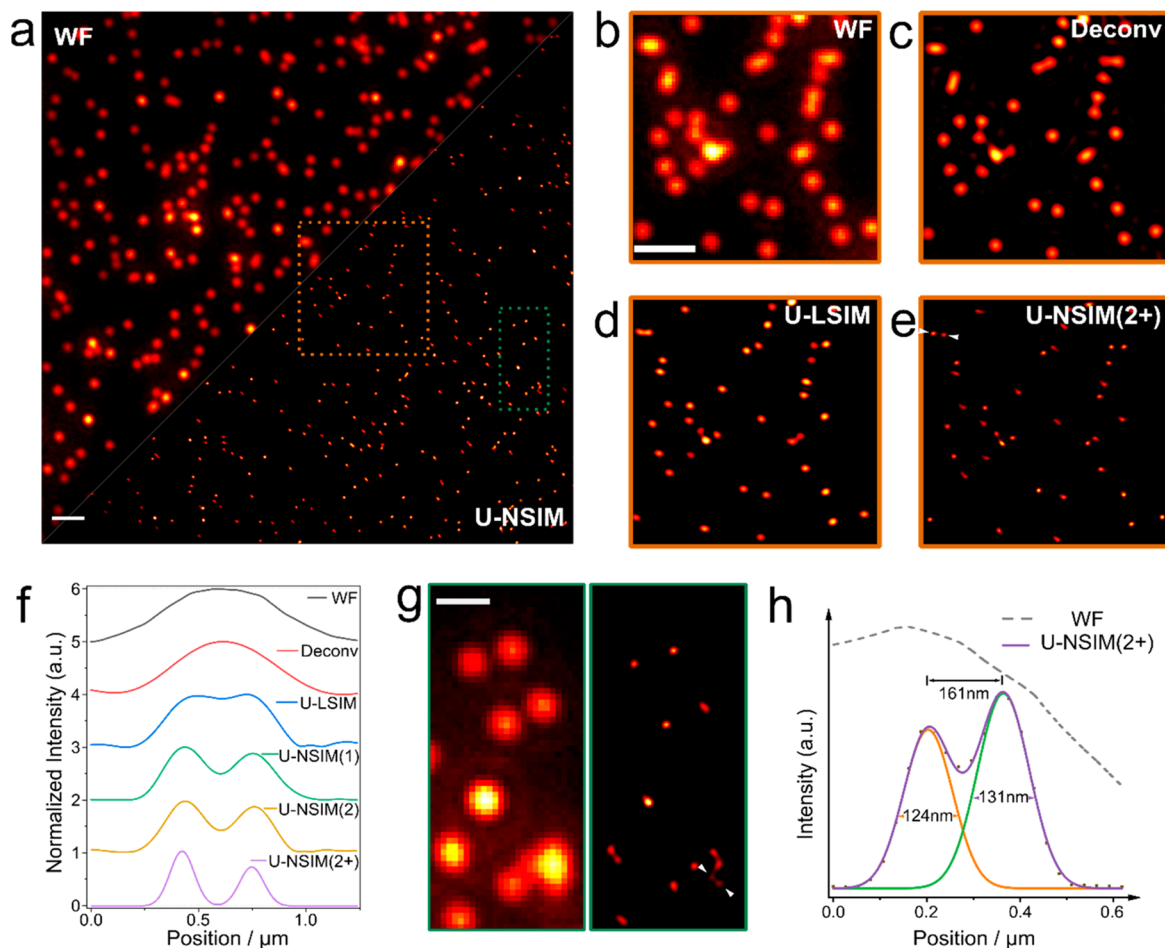


**Figure 3.** Super-resolution imaging reconstructions of upconversion nanocrystals. (a) Wide-field (left) and super-resolution (right) images of the 4% Tm-doped UCNPs. Scale bar: 2  $\mu\text{m}$ . (b–e) Comparison imaging results of a selected area (orange frame) with different imaging modalities: (b) wide-field microscopy; (c) Wiener deconvolution; (d) linear SIM; (e) nonlinear SIM. Scale bar: 2  $\mu\text{m}$ . (f) Line profiles of the resolved particles in the upper-left corner of (e) with a range of imaging methods. (g) Comparison imaging results of the green framed area. (h) Line profiles of two UCNPs at the lower right corner in (g). Scale bar: 1  $\mu\text{m}$ . The diameter of the UCNPs is 40 nm (confirmed by TEM). The reconstruction processes were performed by using both fairSIM<sup>35</sup> in imageJ<sup>36</sup> and a written MATLAB code. The illumination power density is 4  $\text{kW}/\text{cm}^2$ .

emitter doping concentration. A high concentration increases the energy transfer rate from  $\text{Yb}^{3+}$  to  $\text{Tm}^{3+}$  and boosts the cross-relaxation between  $\text{Tm}^{3+}$  ions, thereby enhancing the nonlinearity of the photoresponse. However, a higher doping concentration often leads to lower emission intensity if mild excitation power, e.g., 4  $\text{kW}\cdot\text{cm}^{-2}$ , is used in SIM (Figure 2b). We therefore select the midlevel doping concentration of 4% to compromise between high nonlinearity and high brightness to achieve an optimized imaging quality. We find that the emission intensity can be further improved by tuning the doping concentration of  $\text{Yb}^{3+}$  ions to 40% (Figure 2c), as the optimized  $\text{Yb}^{3+}$  concentration can increase the energy transfer rate from  $\text{Yb}^{3+}$  to  $\text{Tm}^{3+}$ . Figure 2d reveals the resolution-resolving power of nonlinearity for UCNPs with different concentrations by measuring the amplitude of high-frequency harmonics ( $H$ ) in the Fourier transform of their emission pattern (Figure 2d) under a sinusoidal excitation pattern. Compared with the diffraction-limited wide-field imaging result under uniform illumination ( $H = 0$ ) and linear SIM ( $H = 1$ ), the additional harmonics in U-NSIM ( $H \geq 2$ ) improves the lateral resolution to  $\sim \lambda/[2\text{NA}(H + 1)]$ , where NA stands for the numerical aperture.<sup>10,12</sup> Clearly, UCNPs with higher  $\text{Tm}^{3+}$  concentration have stronger harmonic peaks,

with  $H = 3$  for 2% and 4%  $\text{Tm}^{3+}$  and  $H = 4$  for 8%  $\text{Tm}^{3+}$ . Here we identify that 4%  $\text{Tm}^{3+}$  40%  $\text{Yb}^{3+}$  codoped UCNPs are the best suitable probes for U-NSIM, as they provide  $H = 2$  harmonics, while they require lower excitation power than that with 8%  $\text{Tm}^{3+}$  doped UCNPs.

We further examine the resolving power of U-NSIM by resolving single UCNPs on a glass slide (Figure 3). With the schematics of the optical system shown in Supplementary Figure S4, a DMD is used to generate the excitation pattern, and a 60 $\times$  water immersion objective (NA = 1.27) is used to direct excitation and collect the emission (Supplementary Note 4). Figure 3a shows a typical U-NSIM image compared with the diffraction-limited wide-field excitation image across the field of view (FOV) of 32.3  $\mu\text{m} \times 32.3 \mu\text{m}$ , with the comparison images of the 8  $\mu\text{m} \times 8 \mu\text{m}$  area (orange square) by wide-field (WF) microscopy (Figure 3b), Wiener deconvolved result of WF (Figure 3c), upconversion linear SIM (U-LSIM, Figure 3d), and U-NSIM (Figure 3e). To quantify the resolving powers by different modalities, Figure 3f shows the comparison results in resolving a pair of UCNPs separated by a distance of 320 nm, by WF, deconvolution, linear SIM, and nonlinear SIM (Supplementary Figure S5). Here, U-NSIM (1) is reconstructed from 15 raw frames (3

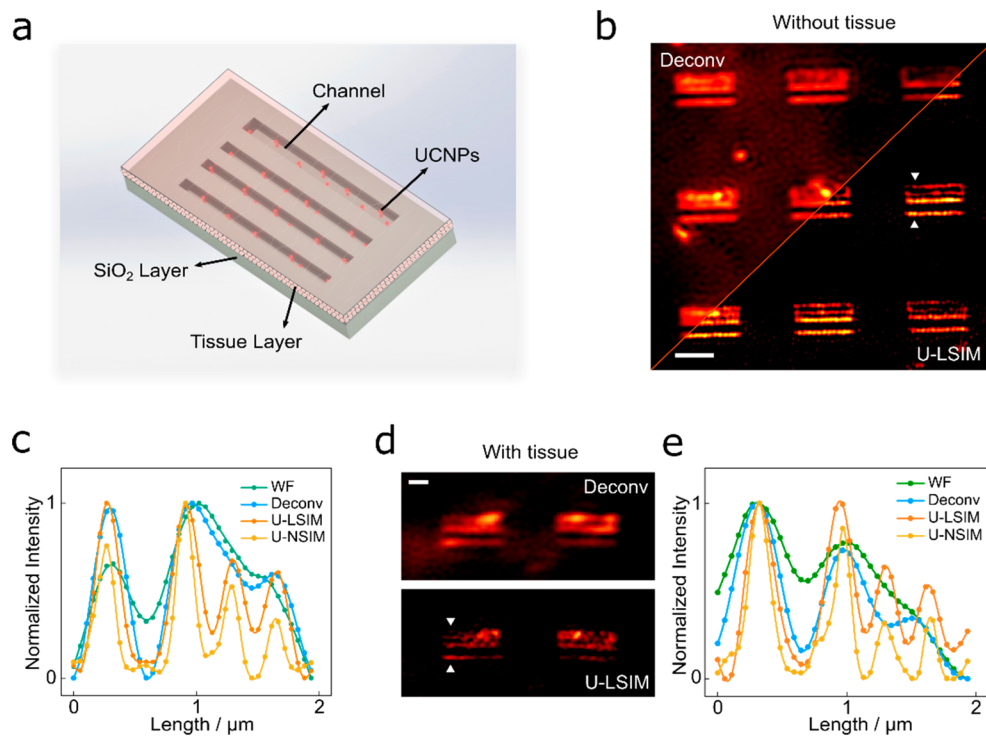


**Figure 4.** Evaluation of the image resolving power of upconversion SIM through thick mouse liver tissue. (a) Schematic diagram of the imaging specimen where the UCNPs are dispersed in the nanochannel structures on a SiO<sub>2</sub> substrate covered with 51.5  $\mu\text{m}$  thick mouse liver tissue. (b) Comparison of images of the specimen by Wiener deconvolution and U-LSIM without covering the tissue slice. The scale bar is 2  $\mu\text{m}$ . (c) Cross section profile of one line in (b) indicated by the white arrows with different methods: wide-field microscopy, Wiener deconvolution, U-LSIM, and U-NSIM. (d) Image of the specimen through a 51.5  $\mu\text{m}$  liver tissue slice by Wiener deconvolution (up) and U-LSIM (bottom). Scale bar is 1  $\mu\text{m}$ . (e) Cross section profile of one line in (d) indicated by the white arrows with different methods. The illumination power density is 4  $\text{kW}/\text{cm}^2$ .

orientations and 5 phase shifts), and U-NSIM (2+) requires 25 raw frames (5 orientations and 5 phase shifts). U-NSIM (2+) stands for NSIM with a Richardson–Lucy deconvolution process (iteration = 10). By imaging another 2.9  $\mu\text{m} \times 6.5 \mu\text{m}$  area (green rectangle), Figure 3h shows that the NSIM modality can resolve two adjacent nanoparticles with a spacing of 161 nm and full width at half-maximum of 124 and 131 nm ( $\sim\lambda_{\text{exc}}/7.5$ ), measured by Gaussian fitting of the line profiles.

Figure 4 further examines the resolving powers of U-LSIM and U-NSIM modalities through thick biological tissues. In this experiment, as shown in Figure 4a, we fabricate nanochannel structures on a SiO<sub>2</sub>/Si substrate (300 nm thermal silicon dioxide layer on top of 500  $\mu\text{m}$  Si) with the line spacing of  $0.35 \pm 0.02$ ,  $0.36 \pm 0.02$ , and  $0.65 \pm 0.02 \mu\text{m}$ , using a standard EBL process. The nanochannels are filled with UCNPs and covered by 51.5  $\mu\text{m}$  thick mouse liver tissue. Figure 4b shows the comparison fluorescence images of the UCNPs stripe pattern using the wide-field (without the tissue cover) and U-LSIM imaging modalities. While the deconvolved wide-field images fail in resolving the stripes below the diffraction limitation ( $\sim 384 \text{ nm}$ ), U-LSIM clearly resolves the stripe pattern. The cross section of the pattern (Figure 4c) demonstrates that the resolution can be further enhanced by U-NSIM. Figure 4d shows the improved resolution of the SIM image through the thick liver tissue, compared with the wide-field image. Due to the reduced extinction of light for NIR wavelength and bright UCNPs emissions, an exposure time of 40 ms per frame is sufficient for U-LSIM to resolve the pattern and an imaging rate of 2.8 Hz for U-LSIM has been achieved. U-NSIM can further increase the resolution and enhance the

signal-to-noise ratio, as shown in Figure 4e, and the imaging rate of 1 Hz has been achieved in this work.

## CONCLUSION

In conclusion, we demonstrate the upconversion nonlinear SIM strategy as a new modality for super-resolution imaging through thick tissue. We find that the nonlinear photoresponse properties of UCNPs can produce high-frequency harmonics in the Fourier domain of the imaging plane, enabling nonlinear SIM with mild excitation power. This work suggests a new scope in probe developments for super-resolution microscopy. The apparent advance by NSIM using UCNPs lies in the improved imaging resolution using the low power CW laser excitation, which can be used for subcellular dynamic tracking of single nanoparticles through deep tissue. Compared with our recent works on single point scanning nanoscopy,<sup>29,34</sup> U-NSIM offers a much higher frame rate. In this work, the excitation power density of 4  $\text{kW}/\text{cm}^2$  at 976 nm only leads to a temperature increase smaller than 3 °C on the tissue sample,<sup>37</sup> which has been approved as safe for long-term single nanoparticle tracking experiment in living cells.<sup>23</sup> Increasing excitation power density can certainly improve the imaging speed, but the high power density may induce a strong photothermal effect. Optimizing the brightness of UCNPs under low power excitation conditions and applying a denoising algorithm, e.g., Hessian deconvolution, to U-NSIM can further improve the imaging speed and resolution. The USIM strategy can be directly adapted to enhance the imaging penetration depth in light sheet based SIM,<sup>38</sup> adaptive optics,<sup>39,17</sup> and reconstruction algorithms.<sup>40</sup> Though specific labeling of UCNPs to the subcellular structures in live cells

remains a challenge, the recent progress with functionalization of UCNPs shows promise in using labeling and single particle tracking to utilize multimodality and multiplexing super-resolution imaging of biomolecules of interest in a live cell environment.<sup>21,33</sup>

## ■ ASSOCIATED CONTENT

### SI Supporting Information

The Supporting Information is available free of charge at <https://pubs.acs.org/doi/10.1021/acs.nanolett.0c00448>.

Nanoparticle synthesis and characterization; TEM images of UCNPs; normalized emission spectrum of UCNPs; illustration of confocal setup; experimental setup of NIR U-SIM; Gaussian fitting of U-NSIM (2+) line profile ([PDF](#))

## ■ AUTHOR INFORMATION

### Corresponding Authors

**Fan Wang** — Institute for Biomedical Materials & Devices (IBMD), Faculty of Science, University of Technology Sydney, Sydney, NSW 2007, Australia; [orcid.org/0000-0001-7403-3305](https://orcid.org/0000-0001-7403-3305); Email: [fan.wang@uts.edu.au](mailto:fan.wang@uts.edu.au)

**Dayong Jin** — Institute for Biomedical Materials & Devices (IBMD), Faculty of Science, University of Technology Sydney, Sydney, NSW 2007, Australia; UTS-SUStech Joint Research Centre for Biomedical Materials & Devices, Department of Biomedical Engineering, Southern University of Science and Technology, Shenzhen 518055, China; Email: [dayong.jin@uts.edu.au](mailto:dayong.jin@uts.edu.au)

### Authors

**Baolei Liu** — Institute for Biomedical Materials & Devices (IBMD), Faculty of Science and School of Mathematical and Physical Sciences, Faculty of Science, University of Technology Sydney, Sydney, NSW 2007, Australia

**Chaohao Chen** — Institute for Biomedical Materials & Devices (IBMD), Faculty of Science, University of Technology Sydney, Sydney, NSW 2007, Australia

**Xiangjun Di** — Institute for Biomedical Materials & Devices (IBMD), Faculty of Science, University of Technology Sydney, Sydney, NSW 2007, Australia

**Jiayan Liao** — Institute for Biomedical Materials & Devices (IBMD), Faculty of Science, University of Technology Sydney, Sydney, NSW 2007, Australia; [orcid.org/0000-0003-0616-4762](https://orcid.org/0000-0003-0616-4762)

**Shihui Wen** — Institute for Biomedical Materials & Devices (IBMD), Faculty of Science, University of Technology Sydney, Sydney, NSW 2007, Australia

**Qian Peter Su** — Institute for Biomedical Materials & Devices (IBMD), Faculty of Science, University of Technology Sydney, Sydney, NSW 2007, Australia

**Xuchen Shan** — Institute for Biomedical Materials & Devices (IBMD), Faculty of Science, University of Technology Sydney, Sydney, NSW 2007, Australia

**Zai-Quan Xu** — School of Mathematical and Physical Sciences, Faculty of Science, University of Technology Sydney, Sydney, NSW 2007, Australia

**Lining Arnold Ju** — School of Biomedical Engineering, Faculty of Engineering and Charles Perkins Centre, The University of Sydney, Camperdown, NSW 2006, Australia; Heart Research Institute, Newtown, NSW 2042, Australia

**Chao Mi** — Institute for Biomedical Materials & Devices (IBMD), Faculty of Science, University of Technology Sydney, Sydney, NSW 2007, Australia; [orcid.org/0000-0003-0895-9948](https://orcid.org/0000-0003-0895-9948)

Complete contact information is available at:  
<https://pubs.acs.org/10.1021/acs.nanolett.0c00448>

### Author Contributions

F.W., B.L., and D.J. conceived the project and designed experiments. B.L., X.S., C.C., and C.M. built the optical setup and performed the optical experiments. J.L. and S.W. synthesized the upconversion nanoparticles. X.D. performed the nanoparticle modification experiment. B.L. and Z.X. prepared the testing samples. Q.S. and L.A.J. prepared the tissue samples. B.L., F.W., and C.C. analyzed the results. B.L., F.W., and D.J. wrote the paper with input from the other authors.

### Notes

The authors declare no competing financial interest.

## ■ ACKNOWLEDGMENTS

This work was supported by the Australian Research Council Discovery Projects (DP190101058, F.W.; DP200101970, L.A.J and Q.P.S.), Sydney Research Accelerator prize (SOAR, L.A.J), Shenzhen Science and Technology Program (KQTD20170810110913065), Australia China Science and Research Fund Joint Research Centre for POCT (ACSRF65827), the Australian Research Council DECRA fellowships (DE200100074, F.W.; DE190100609, L.A.J.), and China Scholarship Council (B.L.: No. 201706020170; C.C.: No. 201607950009; X.D.: No. 201706170028; J.L.: No. 201508530231; X.S.: No. 201708200004). We thank Mr. Chi Li and Mr. Guocheng Fang for their assistance in sample preparations.

## ■ REFERENCES

- (1) Lichtman, J. W.; Conchello, J. A. Fluorescence Microscopy. *Nat. Methods* **2005**, 2 (12), 910–919.
- (2) Eggeling, C.; Willig, K. I.; Sahl, S. J.; Hell, S. W. Lens-Based Fluorescence Nanoscopy. *Q. Rev. Biophys.* **2015**, 48 (2), 178–243.
- (3) Hell, S. W.; Wichmann, J. Stimulated-Emission-Depletion Fluorescence Microscopy. *Opt. Lett.* **1994**, 19 (11), 780–782.
- (4) Rust, M. J.; Bates, M.; Zhuang, X. Sub-Diffraction-Limit Imaging by Stochastic Optical Reconstruction Microscopy (STORM). *Nat. Methods* **2006**, 3 (10), 793–795.
- (5) Betzig, E.; Patterson, G. H.; Sougrat, R.; Lindwasser, O. W.; Olenych, S.; Bonifacino, J. S.; Davidson, M. W.; Lippincott-Schwartz, J.; Hess, H. F. Imaging Intracellular Fluorescent Proteins at Nanometer Resolution. *Science* **2006**, 313 (5793), 1642–1645.
- (6) Dertinger, T.; Colyer, R.; Iyer, G.; Weiss, S.; Enderlein, J. Fast, Background-Free, 3D Super-Resolution Optical Fluctuation Imaging (SOFI). *Proc. Natl. Acad. Sci. U. S. A.* **2009**, 106 (52), 22287–22292.
- (7) Gustafsson, M. G. L. Surpassing the Lateral Resolution Limit by a Factor of Two Using Structured Illumination Microscopy. *J. Microsc.* **2000**, 198 (2), 82–87.
- (8) Wu, Y.; Shroff, H. Faster, Sharper, and Deeper: Structured Illumination Microscopy for Biological Imaging. *Nat. Methods* **2018**, 15 (12), 1011–1019.
- (9) Lal, A.; Shan, C.; Xi, P. Structured Illumination Microscopy Image Reconstruction Algorithm. *IEEE J. Sel. Top. Quantum Electron.* **2016**, 22 (4), 50–63.
- (10) Gustafsson, M. G. L. Nonlinear Structured-Illumination Microscopy: Wide-Field Fluorescence Imaging with Theoretically Unlimited Resolution. *Proc. Natl. Acad. Sci. U. S. A.* **2005**, 102 (37), 13081–13086.

- (11) Rego, E. H.; Shao, L.; Macklin, J. J.; Winoto, L.; Johansson, G. A.; Kamps-Hughes, N.; Davidson, M. W.; Gustafsson, M. G. L. L. Nonlinear Structured-Illumination Microscopy with a Photoswitchable Protein Reveals Cellular Structures at 50-Nm Resolution. *Proc. Natl. Acad. Sci. U. S. A.* **2012**, *109* (3), E135–E143.
- (12) Li, D.; Shao, L.; Chen, B.-C.; Zhang, X.; Zhang, M.; Moses, B.; Milkie, D. E.; Beach, J. R.; Hammer, J. A.; Pasham, M.; et al. Extended-Resolution Structured Illumination Imaging of Endocytic and Cytoskeletal Dynamics. *Science* **2015**, *349* (6251), aab3500.
- (13) Huang, X.; Fan, J.; Li, L.; Liu, H.; Wu, R.; Wu, Y.; Wei, L.; Mao, H.; Lal, A.; Xi, P.; et al. Fast, Long-Term, Super-Resolution Imaging with Hessian Structured Illumination Microscopy. *Nat. Biotechnol.* **2018**, *36* (5), 451–459.
- (14) Guo, Y.; Li, D. D. D.; Zhang, S.; Yang, Y.; Liu, J. J.; Wang, X.; Liu, C.; Milkie, D. E.; Moore, R. P.; Tulu, U. S.; et al. Visualizing Intracellular Organelle and Cytoskeletal Interactions at Nanoscale Resolution on Millisecond Timescales. *Cell* **2018**, *175* (5), 1430–1442.
- (15) Mandula, O.; Kielhorn, M.; Wicker, K.; Krampert, G.; Kleppe, I.; Heintzmann, R. Line Scan-Structured Illumination Microscopy Super-Resolution Imaging in Thick Fluorescent Samples. *Opt. Express* **2012**, *20* (22), 24167–24174.
- (16) Winter, P. W.; York, A. G.; Nogare, D. D.; Ingaramo, M.; Christensen, R.; Chitnis, A.; Patterson, G. H.; Shroff, H. Two-Photon Instant Structured Illumination Microscopy Improves the Depth Penetration of Super-Resolution Imaging in Thick Scattering Samples. *Optica* **2014**, *1* (3), 181–191.
- (17) Zheng, W.; Wu, Y.; Winter, P.; Fischer, R.; Nogare, D. D.; Hong, A.; McCormick, C.; Christensen, R.; Dempsey, W. P.; Arnold, D. B.; et al. Adaptive Optics Improves Multiphoton Super-Resolution Imaging. *Nat. Methods* **2017**, *14* (9), 869–872.
- (18) Kner, P.; Chhun, B. B.; Griffis, E. R.; Winoto, L.; Gustafsson, M. G. L. L. Super-Resolution Video Microscopy of Live Cells by Structured Illumination. *Nat. Methods* **2009**, *6* (5), 339–342.
- (19) Shao, L.; Kner, P.; Rego, E. H.; Gustafsson, M. G. L. Super-Resolution 3D Microscopy of Live Whole Cells Using Structured Illumination. *Nat. Methods* **2011**, *8* (12), 1044–1048.
- (20) Wu, S.; Butt, H. J. Near-Infrared-Sensitive Materials Based on Upconverting Nanoparticles. *Adv. Mater.* **2016**, *28* (6), 1208–1226.
- (21) Jin, D.; Xi, P.; Wang, B.; Zhang, L.; Enderlein, J.; van Oijen, A. M. Nanoparticles for Super-Resolution Microscopy and Single-Molecule Tracking. *Nat. Methods* **2018**, *15* (6), 415–423.
- (22) Zhou, B.; Shi, B.; Jin, D.; Liu, X. Controlling Upconversion Nanocrystals for Emerging Applications. *Nat. Nanotechnol.* **2015**, *10* (11), 924–936.
- (23) Nam, S. H.; Bae, Y. M.; Park, Y. Il; Kim, J. H.; Kim, H. M.; Choi, J. S.; Lee, K. T.; Hyeon, T.; Suh, Y. D. Long-Term Real-Time Tracking of Lanthanide Ion Doped Upconverting Nanoparticles in Living Cells. *Angew. Chem., Int. Ed.* **2011**, *50* (27), 6093–6097.
- (24) Gargas, D. J.; Chan, E. M.; Ostrowski, A. D.; Aloni, S.; Altoe, M. V. P.; Barnard, E. S.; Sanii, B.; Urban, J. J.; Milliron, D. J.; Cohen, B. E.; et al. Engineering Bright Sub-10-Nm Upconverting Nanocrystals for Single-Molecule Imaging. *Nat. Nanotechnol.* **2014**, *9* (4), 300–305.
- (25) Zhao, J.; Jin, D.; Schartner, E. P.; Lu, Y.; Liu, Y.; Zvyagin, A. V.; Zhang, L.; Dawes, J. M.; Xi, P.; Piper, J. A.; et al. Single-Nanocrystal Sensitivity Achieved by Enhanced Upconversion Luminescence. *Nat. Nanotechnol.* **2013**, *8* (10), 729–734.
- (26) He, H.; Liu, B.; Wen, S.; Liao, J.; Lin, G.; Zhou, J.; Jin, D. Quantitative Lateral Flow Strip Sensor Using Highly Doped Upconversion Nanoparticles. *Anal. Chem.* **2018**, *90* (21), 12356–12360.
- (27) Wang, F.; Wen, S.; He, H.; Wang, B.; Zhou, Z.; Shimoni, O.; Jin, D. Microscopic Inspection and Tracking of Single Upconversion Nanoparticles in Living Cells. *Light: Sci. Appl.* **2018**, *7* (4), 18007.
- (28) Liu, Y.; Lu, Y.; Yang, X.; Zheng, X.; Wen, S.; Wang, F.; Vidal, X.; Zhao, J.; Liu, D.; Zhou, Z.; et al. Amplified Stimulated Emission in Upconversion Nanoparticles for Super-Resolution Nanoscopy. *Nature* **2017**, *543* (7644), 229–233.
- (29) Chen, C.; Wang, F.; Wen, S.; Su, Q. P.; Wu, M. C. L.; Liu, Y.; Wang, B.; Li, D.; Shan, X.; Kianinia, M.; et al. Multi-Photon near-Infrared Emission Saturation Nanoscopy Using Upconversion Nanoparticles. *Nat. Commun.* **2018**, *9*, 3290.
- (30) Bednarkiewicz, A.; Chan, E. M.; Kotulska, A.; Marciniak, L.; Prorok, K. Photon Avalanche in Lanthanide Doped Nanoparticles for Biomedical Applications: Super-Resolution Imaging. *Nanoscale Horizons* **2019**, *4* (4), 881–889.
- (31) Zhan, Q.; Liu, H.; Wang, B.; Wu, Q.; Pu, R.; Zhou, C.; Huang, B.; Peng, X.; Ågren, H.; He, S. Achieving High-Efficiency Emission Depletion Nanoscopy by Employing Cross Relaxation in Upconversion Nanoparticles. *Nat. Commun.* **2017**, *8*, 1058.
- (32) Peng, X.; Huang, B.; Pu, R.; Liu, H.; Zhang, T.; Widengren, J.; Zhan, Q.; Ågren, H. Fast Upconversion Super-Resolution Microscopy with 10  $\mu$ s per Pixel Dwell Times. *Nanoscale* **2019**, *11* (4), 1563–1569.
- (33) Zeng, X.; Chen, S.; Weitemier, A.; Han, S.; Blasiak, A.; Prasad, A.; Zheng, K.; Yi, Z.; Luo, B.; Yang, I.; et al. Visualization of Intra-Neuronal Motor Protein Transport through Upconversion Microscopy. *Angew. Chem., Int. Ed.* **2019**, *58* (27), 9262–9268.
- (34) Liu, Y.; Wang, F.; Lu, H.; Fang, G.; Wen, S.; Chen, C.; Shan, X.; Xu, X.; Zhang, L.; Stenzel, M.; et al. Super-Resolution Mapping of Single Nanoparticles inside Tumor Spheroids. *Small* **2020**, *16*, 1905572.
- (35) Müller, M.; Mönkemöller, V.; Hennig, S.; Hübner, W.; Huser, T. Open-Source Image Reconstruction of Super-Resolution Structured Illumination Microscopy Data in ImageJ. *Nat. Commun.* **2016**, *7*, 10980.
- (36) Schneider, C. A.; Rasband, W. S.; Eliceiri, K. W. NIH Image to ImageJ: 25 Years of Image Analysis. *Nat. Methods* **2012**, *9* (7), 671–675.
- (37) Crane, N. J.; Huffman, S. W.; Gage, F. A.; Levin, I. W.; Elster, E. A. 980-Nm Infrared Laser Modulation of Sodium Channel Kinetics in a Neuron Cell Linearly Mediated by Photothermal Effect. *J. Biomed. Opt.* **2014**, *19* (10), 105002.
- (38) Chen, B.-C. B. C.; Legant, W. R.; Wang, K.; Shao, L.; Milkie, D. E.; Davidson, M. W.; Janetopoulos, C.; Wu, X. S.; Hammer, J. A.; Liu, Z.; et al. Lattice Light-Sheet Microscopy: Imaging Molecules to Embryos at High Spatiotemporal Resolution. *Science* **2014**, *346* (6208), 1257998.
- (39) Kner, P.; Wolstenholme, A.; Chaudhari, S. N.; Kipreos, E. T.; Thomas, B. Enhanced Resolution through Thick Tissue with Structured Illumination and Adaptive Optics. *J. Biomed. Opt.* **2015**, *20* (2), 026006.
- (40) Jost, A.; Tolstik, E.; Feldmann, P.; Wicker, K.; Sentenac, A.; Heintzmann, R. Optical Sectioning and High Resolution in Single-Slice Structured Illumination Microscopy by Thick Slice Blind-SIM Reconstruction. *PLoS One* **2015**, *10* (7), No. e0132174.